Origin of ferromagnetism in ZnO codoped with Ga and Co: Experiment and theory

Y. He,[1] Parmanand Sharma,[2] Krishanu Biswas,[3] E. Z. Liu,[1] Naofumi Ohtsu,[2] A. Inoue,[2] Y. Inada,[4] M. Nomura,[4] J. S. Tse,[1,5]
S. Yin,[1] and J. Z. Jiang[1,*]

[1]*International Center for New-Structured Materials (ICNSM), Zhejiang University, Hangzhou 310027, People's Republic of China
and Laboratory of New-Structured Materials, Department of Materials Science and Engineering, Zhejiang University,
Hangzhou 310027, People's Republic of China*
[2]*Institute for Materials Research, Tohoku University, 2-1-1 Katahira, Aoba-Ku, Sendai, 980-8577, Japan*
[3]*Department of Materials and Metallurgical Engineering, Indian Institute of Technology,
Kanpur -208016, U. P., India,*
[4]*High Energy Accelerator Research Organization, Institute of Materials Structure Science, Photon Factory, Oho 1-1,
Tsukuba 305-0801, Japan*
[5]*Department of Physics and Engineering Physics, University of Saskatchewan, Saskatoon, Canada S7N 5E2*

In view of the recent controversies on the above room-temperature ferromagnetism in pure ZnO and the transition-metal doped ZnO, the present paper aims to shed some light on the origin of ferromagnetism by investigating the detailed atomic structure of (Co, Ga)-codoped ZnO experimentally as well as theoretically. Above room-temperature ferromagnetism in nonmagnetic Co-doped ZnO, nanoparticle powders prepared by sol-gel technique were obtained by codoping with Ga. It is found that Co ions substitute Zn sites while Ga ions were located at octahedral interstitial sites together with one O vacancy. Electrons from the Ga $4p^{\uparrow}$ states transform to the unfilled Co $3d^{\downarrow}$ states. The strong hybridization between the charge carriers in the Co $3d$ and Ga $4p$ states and electronic polarization for surrounding O ions at Co ions are detected. Finally, the Ga-$4p$ electrons merged with conduction band and polarized O ions act as medium for an indirect exchange between the Co ions, which could be the origin of ferromagnetism in the (Co, Ga)-codoped ZnO.

I. INTRODUCTION

In the field of spintronics, it is essential to develop semiconductors with ferromagnetically polarized carriers at room temperature (RT) such that the spin as well as charge of the carriers can be coupled with an external magnetic field to control devices. Fascination toward the development of such materials is due to their tremendous application potential, which will have a huge effect on our day to day life. For example, such types of material will be capable of integrating the electronics, magnetism, and optical functionalities in a single material, leading to low cost, high-speed, and small sized devices operating at very low power. The theoretical prediction of such materials, "so-called diluted magnetic semiconductor (DMS)," operational at RT by Dietl *et al.*[1] has stimulated several experimental groups, which resulted in the production of magnetic semiconductors in the various host semiconductor materials (such as ZnO, TiO₂, and In₂O₃) by doping with $3d$ transition metals.[2–4] For most of the experimental results, doubts arose about the real origin of ferromagnetism (FM). For some cases, it was demonstrated that the ferromagnetism is due to segregation of metallic clusters while in some systems it is because of the transition-metal elements with different valence states. Recently, it was reported that the host material itself (without any magnetic element doping) becomes magnetic when the size of the crystallites is in nanometers.[5,6] The capping of organic molecules onto the host nanoparticles without any magnetic impurities can also modify the electronic structure, giving rise to FM-like behavior at RT.[6] Besides FM with Curie temperatures ranging from low temperature to several hundred degrees Celsius above RT, many groups reported the same materials as spin glass or even nonmagnetic. These controversial results suggest that it is challenging to identify particular atomic structure and electronic configuration, which are responsible for the magnetism in such system and can open a world of possibilities for their proper use in the field of spintronics. In the present work, we uncover some of the facts about the atomic and electronic structures of (Co, Ga)-codoped ZnO DMS.

Subsequent to the early work on high-temperature FM in Co-doped ZnO by Ueda *et al.*,[7] a number of groups reported similar results.[8–13] As mentioned above, antiferromagnetic (AFM), nonmagnetic, and spin-glass behaviors were also reported.[11–13] These controversial results led to a debate about the origin of FM in Co-doped ZnO.[14–27] Mechanism based on free charge carrier inducing Ruderman-Kittel-Kasuya-Yosida (RKKY)-like interactions has been proposed by Dietl *et al.*[1] However, Khare *et al.*[17] reported that the introduction of large number of carriers in Co-doped ZnO have no effect on the FM. The RT FM is due to coupling between $3d$ transition-metal impurities and localized charge carriers (shallow donor electrons), supporting the impurity-band exchange mechanism proposed by Coey *et al.*[18] On the other hand, Sluiter *et al.*[19] showed that the nonmagnetic Co-doped ZnO becomes ferromagnetic with the codoping of Li (which introduces the extra holes) and the RT magnetization increases as the Li concentration increases. Recently, similar results were also reported by Liu *et al.*[20] by codoping with Al. These results along with the magneto-optical measurements on this system pointed out that the FM is carrier induced.[21–24] Again, Alaria *et al.*[25] reported that Al-doped $Zn_{0.9}Co_{0.1}O$ showed no ferromagnetic properties in spite of

the creation of free carriers. Recently, Behan *et al.*[26] showed that there are two distinct ferromagnetic mechanisms in doped ZnO by varying carrier densities (e.g., produced by Al): magnetic polarons and carrier-mediated exchange. At low carrier densities, magnetic polarons give rise to ferromagnetism for the poor conducting films. At high carrier densities, the magnetization depends on the carrier density, as predicted by the theory of carrier-mediated exchange. Thus, the origin of FM still remains controversial. To understand the origin of FM in such system, one has to determine the crystallographic and electronic structures of Co^{2+} ions and the codoped ions (Al, Li). X-ray absorption fine-structure (XAFS) technique, which is a species-specific tool providing local coordination information, can reveal the local structure[27] but it is difficult for Al and Li ions. In the present study, we substituted Al with Ga and successfully synthesized homogeneous (Co, Ga)-codoped ZnO, exhibiting room-temperature FM.

II. EXPERIMENT

The Co-doped and (Co, Ga)-codoped ZnO powders were prepared from the acetate-derived precursors using the sol-gel route. $Zn(CH_3COO_2)_2 \cdot 2H_2O$ (99.9%), $Co(CH_3COO_2)_2 \cdot 4H_2O$ (99.9%), and $GaCl_3$ (99.999%) were first dissolved in a mixture of monoethanolamine (MEA) and 2-methoxyethanol at room temperature. The concentration of doping ions was designed in such a way that the molar ratio of MEA to metal cations in the solution was kept at 2 and the concentration of total metal cations in the solution was 0.7 mol/l. The precursory solution was stirred at 70 °C for 1 h to yield a purple solution in an alumina crucible. The solution in the alumina crucible was then heated in a furnace at 125 °C for 1 h to evaporate the solvent and then kept at 300 °C for 2 h to remove organic residuals. The powders were annealed at 500 °C for 30 min. The powders were green after annealing. Lastly, the green powders were washed using alcohol and centrifuged three times, and then dried at 70 °C.

The structural analysis of the Co-doped ZnO and (Co, Ga)-doped ZnO powders was carried out by x-ray diffraction (Rigaku RINT—Ultima III, Cu $K\alpha$ radiation with accelerating voltage and current of 40 kV and 40 mA, respectively) and high-resolution transmission electron microscopy (HR-TEM) (FEI Technai G^2, accelerated at 300 kV) with x-ray energy-dispersive spectroscopy (EDS) (Oxford make). Magnetic properties were characterized by using a superconducting quantum interference device (SQUID) magnetometer (Quantum Design MPMSR 5*s*). The electronic structural measurements of Co and Ga atoms in the samples were performed using x-ray photoelectron spectroscopy (XPS). XAFS measurements, used to determine the atomic location of dopants, were performed on beamline BL12C at the KEK Synchrotron Radiation Facility in Japan.

In first-principles calculations, we first used ground-state density-functional theory (DFT) calculations to relax the Co-doped ZnO lattice with Ga ions at different positions, and then used these relaxed coordinates as input to the *ab initio* real-space full multiple-scattering code FEFF8 for the calcu-
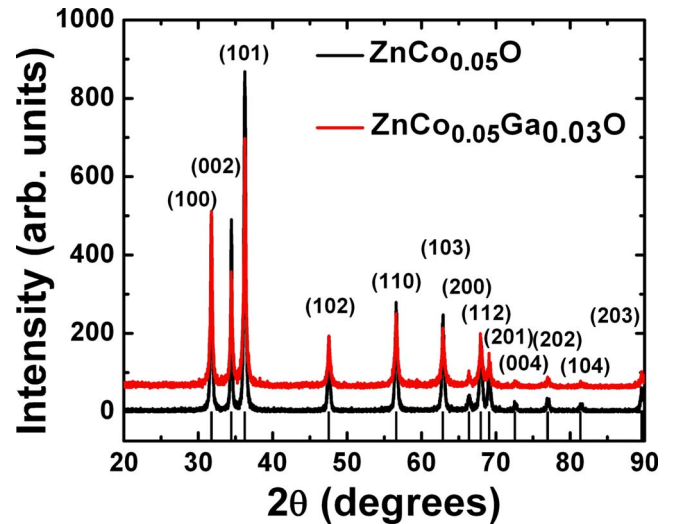

FIG. 1. (Color online) X-ray diffraction patterns of Co-doped ZnO and (Co, Ga)-codoped ZnO. All the peaks match with the XRD pattern of pure ZnO. The lines on the *x* axis correspond to the peak positions for the pure ZnO.

lation of the simulated x-ray absorption spectra.[28] Our total energy and electronic structure calculations were performed using the projector augmented wave[29] (PAW) formalism of density-functional theory, as implemented in the VASP package.[30] The default VASP PAW potentials with 12 valence electrons for Zn ($3d^{10}4s^2$), six for O ($2p^42s^2$), nine for Co ($3d^8s^1$), and three for Ga ($4s^24p^1$) were used. We used an energy cutoff of 500 eV for plane-wave expansion of the PAWs. The exchange-correlation functional is approximated with the fully localized limit of the local spin-density approximation (LSDA)$+U$ method.[31] Here we use typical values of $U=5$ eV on Co atoms.[32] In order to achieve realistic experimental dopant concentrations ($\sim$5% Co and $\sim$3% Ga), we used a periodic $3 \times 3 \times 2$ wurtzite supercell of ZnO, which consists of 72 atoms in a unit cell and substitute two Co ions for two Zn atoms. We found that the two Co ions with the nearest distance are the most stable configuration. The Brillouin zone is sampled using a $3 \times 3 \times 2$ Γ-centered *k*-point grid. For all geometry optimizations, we allowed the volume of the supercell to be relaxed, as well as all the internal coordinates, until the Hellmann-Feynman forces were less than 0.01 eV/Å.

III. RESULTS AND DISCUSSION

Figure 1 shows the x-ray diffraction (XRD) patterns of 5 at % Co-doped ZnO (marked as $Zn_{0.95}Co_{0.05}O$) together with 3 at % Ga codoped (marked as $Zn_{0.92}Co_{0.05}Ga_{0.03}O$) powders. All the peaks correspond to ZnO-like phase with a wurtzite structure (space-group $P6_3/mmc$). No secondary phases can be detected on the resolution of XRD. However, x-ray diffraction is insensitive to small precipitates of any impurities. Thus, we cannot confirm the absence of Co or Ga metal clusters or oxides if they are present in small quantity while being detected by XRD. Thus, HRTEM measurements were performed. The low magnification image of the par-
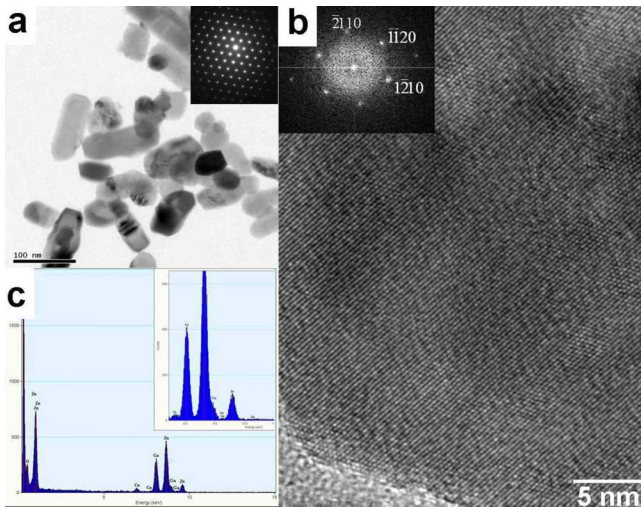
FIG. 2. (Color online) Transmission electron microscopic observations of $Co_{0.05}Zn_{0.92}Ga_{0.03}O$: (a) bright field image showing nanoparticles with inset showing selected area diffraction pattern (SADP) from one such particle, (b) atomic resolution image showing absence of second phase or segregation of Co or Ga with inset showing FFT of the image, and (c) EDS pattern obtained from the particle with inset showing zoom of the portion indicated in the figure

ticles of $Zn_{0.92}Co_{0.05}Ga_{0.03}O$ is shown in Fig. 2(a). It clearly reveals the presence of nanometer-sized (40–200 nm) particles. The inset of Fig. 2(a) shows selected area diffraction pattern from one such particle along [0001] direction, revealing wurtzite crystal structure. Figure 2(b) shows atomic resolution image obtained from one of those nanometer-sized particles with inset showing fast Fourier transform (FFT) of the high-resolution image. No secondary phases (oxides) or clustering of Co or Ga in the particle were detected. FFT confirms the wurtzite structure of the particle. In addition, FFT patterns obtained from about 20 high-resolution images

do not reveal any diffraction spot corresponding to second phase. In order to confirm the presence of different elements in the nanometer-sized particles, Fig. 2(c) shows EDS pattern from the same particle in Fig. 2(b), revealing the presence of Zn, O, Co, and Ga. The Cu peaks are due to the carbon coated Cu grid, which is used to mount the samples in transmission electron microscopy (TEM) sample holder. Similar results were also obtained for $Zn_{0.95}Co_{0.05}O$ and $Zn_{0.95}Co_{0.05}Ga_{0.01}O$. Thus, XRD and HRTEM results indicate that the presence of any second phase or segregation could not be detected in the investigated particles in the samples studied.

The dc magnetic-field-dependent magnetization curves $M(H)$ for $Zn_{0.95}Co_{0.05}O$ and $Zn_{0.92}Co_{0.05}Ga_{0.03}O$ powders recorded at 5 and 300 K are shown in Figs. 3(a) and 3(b). A linear variation in magnetization with field can be noticed in the case of $Zn_{0.95}Co_{0.05}O$, indicating the absence of FM [Fig. 3(a)], which is consistent with our previous results.[21] Introduction of only 3 at % of Ga resulted in a drastic change in the $M(H)$ curve shape in Fig. 3(b). S-shaped curves with a finite value of coercivity (H_c) and remanence (M_r) were obtained at 5 and 300 K ($H_{c5K} \sim 672$ Oe $M_{r5K} \sim 408$ emu/mole Co; $H_{c300K} \sim 555$ Oe, $M_{r300K} \sim 248$ emu/mole Co), indicating that $Zn_{0.92}Co_{0.05}Ga_{0.03}O$ is ferromagnetic with the Curie temperature above RT. It is found that the value of H_c is high in the present case as compared to other DMS systems ($H_c \sim 100$ Oe). The origin for high H_c is not clear yet. Appreciable difference in the temperature dependent dc susceptibility (χ) measured in the zero-field cooled (ZFC) and field cooled (FC) states under low magnetic fields (of 500 and 1000 Oe) was observed for $Zn_{0.92}Co_{0.05}Ga_{0.03}O$ [Fig. 3(d)]. However, we did not observe such difference in ZFC and FC for $Zn_{0.95}Co_{0.05}O$ [Fig. 3(c)]. The temperature dependent susceptibility is similar to the paramagnetic materials. The temperature dependence of χ for paramagnetic materials is governed by the Curie-Weiss law,
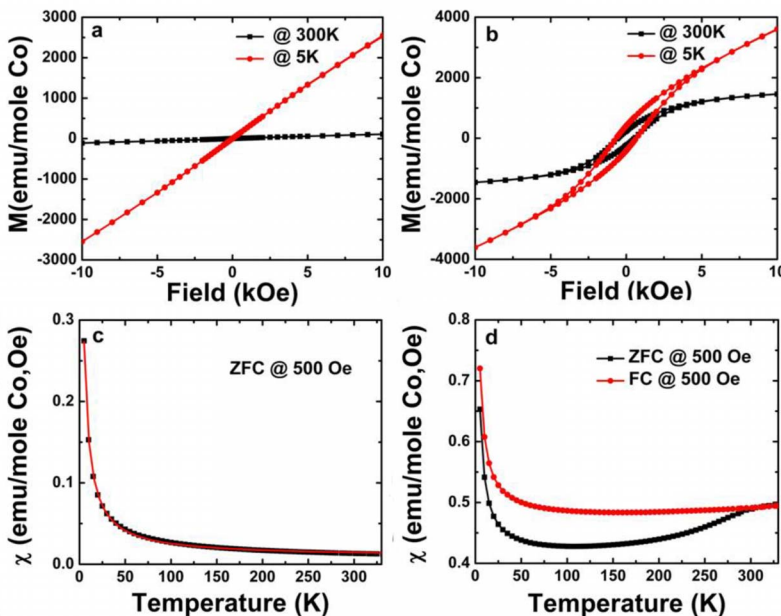

FIG. 3. (Color online) (a) Hysteresis loops for $Zn_{0.95}Co_{0.05}O$ sample measured at 5 and 300 K, and (b) hysteresis loops for $Zn_{0.92}Co_{0.05}Ga_{0.03}O$ sample measured at 5 and 300 K. Temperature-dependent magnetization in the ZFC and FC states measured by applying a magnetic field of 500 Oe (c) for $Zn_{0.95}Co_{0.05}O$ sample, where both the ZFC and FC curves completely coincide with each other, and (d) for $Zn_{0.92}Co_{0.05}Ga_{0.03}O$ sample showing a significant difference in the ZFC and FC curves. The red line in Fig. 3(c) is the Curie-Weiss fitting curve.

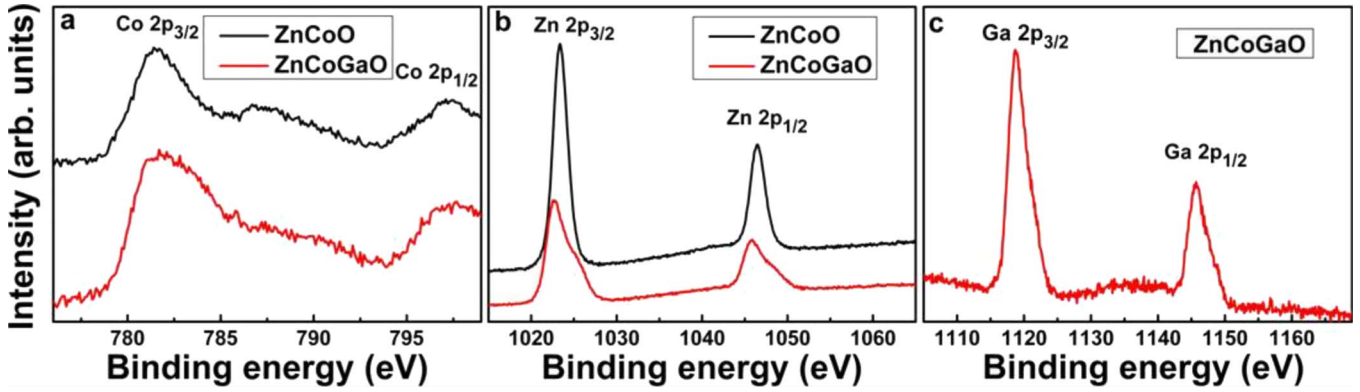FIG. 4. (Color online) (a) Co and (b) Zn $2p$ core-level XPS spectra for $Zn_{0.95}Co_{0.05}O$ and $Zn_{0.92}Co_{0.05}Ga_{0.03}O$ samples, and (c) Ga $2p$ core-level XPS spectra for $Zn_{0.92}Co_{0.05}Ga_{0.03}O$ sample.

$$\chi = \chi_0 + \frac{C}{(T - \Theta)}, \quad C = \frac{N_A \mu^2}{3k_B}, \quad (1)$$

where C is Curie constant, μ is magnetic moment, N_A $=6.0221 \times 10^{23}$ mol^{-1} is the Avogadro number, $k_B = 1.3807 \times 10^{-16}$ erg K^{-1} is Boltzmann's constant. The χ vs T data for $Zn_{0.95}Co_{0.05}O$ was fitted by Eq. (1) [Fig. 3(c)] and gives $C = 1.65$ emu K/mol Co, $\Theta = -1.25$ K. The negative value of Θ is usually observed in the case of local atomic antiferromagnetic interaction. The value μ for Co^{2+} can be estimated from Eq. (1). The calculated value of $\mu = 3.6\mu_B$/Co is close to the expected value of $\mu = 4.8\mu_B$ for high-spin Co^{2+}. This value is calculated for $x = 0.05$ (5% doping of Co in ZnO); any deviations from this nominal value may account for the observed discrepancies. These magnetic characteristics indicated that the Ga doping turned nonmagnetic Co-doped ZnO into magnetic at RT.

The magnetism in Co-doped ZnO reported in literature could be the result of Co segregation or the effect of defected structure of the host ZnO nanoparticles, which itself behaves like a ferromagnet. However, these possibilities can be ruled out in the present work. The nonmagnetic behavior of pure Co-doped ZnO observed here, together with XRD and HR-TEM results mentioned above, indicate absence of any metallic Co segregation, which is consistent with our previous work.[27] The saturation magnetization of the host ZnO nanoparticles or the defect induced magnetization in ZnO is of the order of $\sim 10^{-3}$ emu/g,[5,6] which is negligible as compared to ~ 0.9 emu/g (~ 1458 emu/mole Co) obtained in the present study for the (Co, Ga)-codoped ZnO. The magnetic properties of (Co, Ga)-codoped ZnO samples are similar to (Co, Li)-codoped ZnO, where Li doping induce room-temperature FM in nonmagnetic Co-doped ZnO.[19] However, the RT magnetization under the magnetic field of 1 T for $Zn_{0.92}Co_{0.05}Ga_{0.03}O$ is an order of magnitude higher ($M_{s@1T}$ ~ 1458 emu/mol Co) than the $Zn_{0.90}Co_{0.05}Li_{0.05}O$ ($M_{s@1T}$ ~ 97 emu/mol Co), indicating Ga is a better choice for codoping. Also $M_s = xN_A$, using $M_{s1T} = 1458$ emu/mol Co, $x = 0.05$ yields $\mu = 0.26\mu_B$/Co site for $Zn_{0.92}Co_{0.05}Ga_{0.03}O$ sample. This value of μ is considerably smaller than $\mu = 1.7\mu_B$ for metallic Co^0. However, it is common that only fraction of Co spins contributes to the ferromagnetism and

the rest of the spins are still in paramagnetic state in diluted magnetic semiconductors. This is well supported by the existence of strong exponential increase in magnetization similar to nonmagnetic Co-doped ZnO (Fig. 3). The low-temperature part ($\sim$ up to 150 K) of field cooled χ vs T curve shown in Fig. 3(d) can be fitted to the Curie-Weiss law [Eq. (1)], giving $C = 1.46$ emu K/mol. It is worth pointing out that the shape of the χ (or magnetization) vs T curve measured under an in-plane magnetic field of 1 T for $Zn_{0.92}Co_{0.05}Ga_{0.03}O$ is similar to the $Zn_{0.95}Co_{0.05}O$. Fit to the Curie-Weiss law gives $C = 1.46$ emu K/mol, which is exactly the same obtained in case of measurement performed under low magnetic field [Fig. 3(d)].

To understand the mechanism of FM in $Zn_{0.92}Co_{0.05}Ga_{0.03}O$, the local crystallographic and electronic structures of the Co and Ga dopants in the samples were characterized by x-ray photonelectronic spectroscopy (XPS) and XAFS together with first-principles calculations. Figure 4(a) shows the Co $2p$ core-level XPS spectra of $Zn_{0.95}Co_{0.05}O$ and $Zn_{0.92}Co_{0.05}Ga_{0.03}O$ samples. Comparison of the shapes and positions of peaks for the two samples with standards (metallic Co, CoO, and γ-Co_2O_3 in Ref. 22) reveals that Co ions in the samples are indeed Co^{2+} valence, while no indication of Co^0 and Co^{3+} ions were detected within the resolution of the technique. The spectra are characterized by a Co $2p_{3/2}$ peak at ca. 781.7 eV and a Co $2p_{1/2}$ peak at ca. 797.2 eV for $Zn_{0.95}Co_{0.05}O$. Similar binding energies of these peaks are found in $Zn_{0.92}Co_{0.05}Ga_{0.03}O$ sample. The difference between the binding energies of these peaks is about 15.5 eV consistent with CoO,[33,34] indicating that Co ions in both samples are in high-spin divalent state. Broadening of Co $2p$ core-level is detected in $Zn_{0.92}Co_{0.05}Ga_{0.03}O$ sample, as compared to $Zn_{0.95}Co_{0.05}O$ sample, which indicates the existence of interaction between Ga and Co ions. The Zn $2p$ core-level XPS spectra of two samples are shown in Fig. 4(b). The binding energy of the Zn_{2p} electron in $Zn_{0.95}Co_{0.05}O$ is about 2.3 eV higher than that in pure ZnO,[35] indicating the decrease in valence electron density of Zn ions. This shift most likely resulted from the high electronegativity of Co (~ 1.88), which is higher than that of Zn (~ 1.65). The valence electron density of Zn in the Zn-O-Co bond in $Zn_{0.95}Co_{0.05}O$ should be lower than that in the Zn-O-Zn bond in pure ZnO. Interestingly, it is
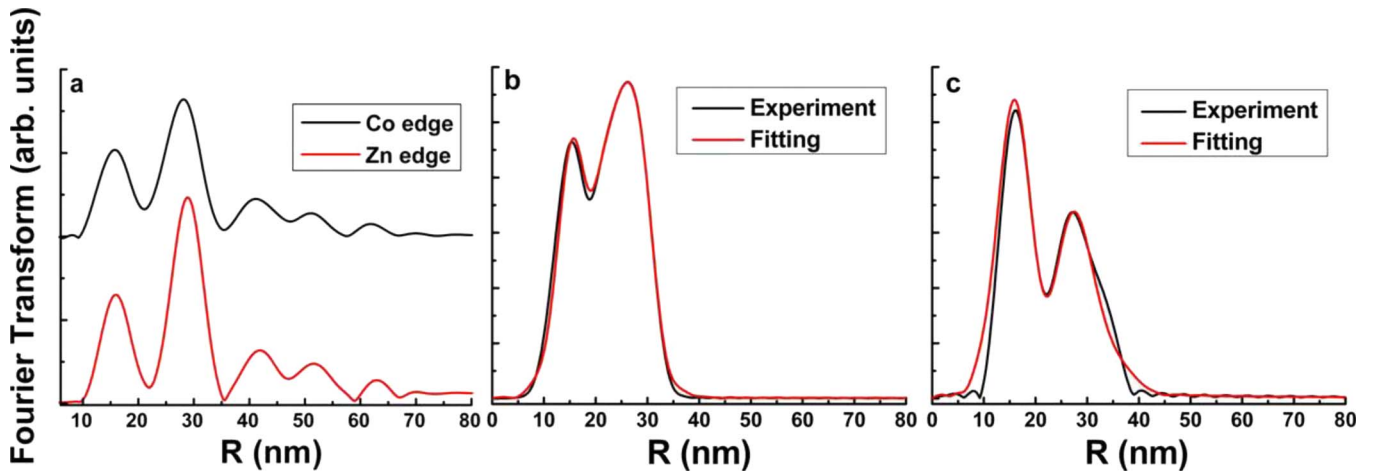
FIG. 5. (Color online) Fourier transforms of the experimental (a) Co K-edge and Zn K-edge XAFS signals for $Zn_{0.95}Co_{0.05}O$ sample. Fourier transforms of the experimental (b) Co K-edge and (c) Ga K-edge XAFS signals for $Zn_{0.92}Co_{0.05}Ga_{0.03}O$ sample.

found that the binding energy of the Zn_{2p} electron decreases with doping Ga into $Zn_{0.95}Co_{0.05}O$, as shown in Fig. 4(b). This result strongly suggests that Ga doping does affect the electronic structure of Zn ions. Assuming that a Zn-O-Ga bond is formed, the binding energy of the Zn_{2p} electron should increase but the fact is opposite. The decrease suggested a compensation effect for the valence electron density of Zn for the presence of Ga atoms, i.e., interaction between Co and Ga, which causes the binding energy of the Zn_{2p} electron shifts, but that the Co_{2p} electron does not. A "shoulder" on the right side of the Zn $2p_{3/2}$ peak is observed for $Zn_{0.92}Co_{0.05}Ga_{0.03}O$ sample. This is presumably due to the Zn ions having defects as nearest neighbors in the sample. These defects might be O vacancies and interstitial Ga ions (details are given below). Ga ions in the samples are indeed Ga^{3+} valence by comparing the shapes and positions of peaks for the sample in Fig. 5(c) with standard Ga_2O_3.[36] The binding energy of Ga $2p_{3/2}$ peak at ca. 1118.8 eV is about 0.9 eV higher than that of pure Ga_2O_3. This reveals a decrease in the valence electron density of Ga, which may be caused by electron transformation from the host Ga $4p^{\uparrow}$ states to the unfilled Co $3d^{\downarrow}$ states. A similar explanation was also reported in Ref. 34. This interaction could strongly link with the high-temperature FM in $Zn_{0.92}Co_{0.05}Ga_{0.03}O$ sample.

Figure 5(a) shows the radial distribution function (RDF), i.e., Fourier transform amplitude of Co K-edge and Zn K-edge XAFS spectra for $Zn_{0.95}Co_{0.05}O$ sample, respectively. It is clear that the atomic environment of Co is similar to that for Zn in $Zn_{0.95}Co_{0.05}O$ sample, indicating that Co ions do substitute for Zn ions in the wurtzite ZnO lattice, which is consistent with our previous study.[27] Figs. 5(b) and 5(c) show the Fourier transforms of the Co K-edge and Ga K-edge XAFS spectra for $Zn_{0.92}Co_{0.05}Ga_{0.03}O$ sample together with FEFF (Ref. 37) fits. It is found that although Co ions also substitute for Zn ions in the wurtzite ZnO lattice, difference in RDF between $Zn_{0.95}Co_{0.05}O$ and $Zn_{0.92}Co_{0.05}Ga_{0.03}O$ is detected, which is caused by the presence of Ga ions in the latter. Several atomic models were considered to fit the Ga K-edge XAFS pattern, i.e., (1) substitution site and (2) interstitial sites. After many trials, we found that it is impossible to get a reasonable fit to XAFS

data when one assigns Ga ions at substitution sites. For interstitial sites, a few atomic models were further considered, such as, presence of vacancy of Zn or O and tetrahedral interstitial site or octahedral interstitial site. The final atomic model is found, as shown in Fig. 6(a), in which two Co ions are located at Zn sites along a-b plane in the wurtzite structure. Ga ions are located at octahedral interstitial sites together with one O vacancy. This atomic model can simultaneously fit both Co K-edge and Ga K-edge XAFS spectra well for $Zn_{0.92}Co_{0.05}Ga_{0.03}O$ sample in Figs. 5(b) and 5(c). The first-shell Co-O is composed of about 3 ± 0.5 oxygen ions, located at 1.96 Å. The substitution of Co results in the contraction of the first shell around the Co to be in agreement with the slight small radius of Co^{2+}, as compared to Zn ions. For pure ZnO, four O ions are located around Zn ions. The decrease in the first-shell coordination number of Co indicates the presence of O vacancies in (Co, Ga)-codoped ZnO sample. The fit further reveals a second-shell coordination of 2 ± 0.5 Zn and Co atoms at 2.51 Å, a third-shell coordination of 1 ± 0.5 Ga atoms at 2.79 Å, and a fourth-shell coordination of 5 ± 0.5 Zn and Co atoms at 3.19 Å. However, only from XAFS data, we are not able to determine the exact coordination number of Zn and Co ions separately. Around Ga ions, we found (1) Ga-O at 2.51 Å with coordination number of about 3.3 ± 0.5 and at 3.49 Å with coordination number of 1. We also found (2) Ga-Zn at 2.43 Å with coordination number of about 2.2 ± 0.5, at 2.94 Å with coordination number of 2.6 ± 0.5, and at 3.47 Å with coordination number of 1. Furthermore, we found (3) Ga-Co at 2.69 Å with coordination number of about 1.4 ± 0.5. Based on the atomic structure in Fig. 6(a), thus, it is not unreasonable to explain the shoulder in the Zn $2p$ core-level XPS spectra in Fig. 4(b) for Zn ions surrounded by Ga ions at interstitial sites and O vacancies in $Zn_{0.92}Co_{0.05}Ga_{0.03}O$ sample.

In the first-principles calculations, using the atomic model illustrated in Fig. 6(a), it is found that the FM configuration of the system [Fig. 6(a)] is more stable by 0.75 eV than AFM configuration. The coupling appears rather strong, which is consistent with experimental observation in Fig. 3. To further understand the origin of the high-temperature FM, density of states (DOS) and electronic structure of the system were
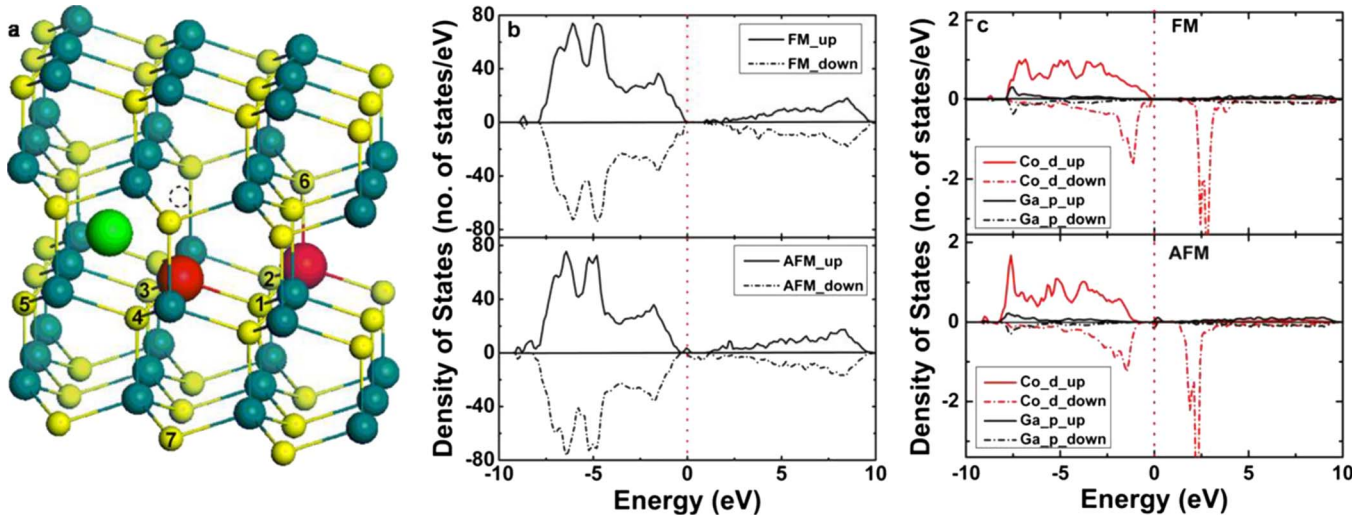
FIG. 6. (Color online) (a) The atomic structure for (Co, Ga)-doped ZnO with O vacancies. The blue, yellow, red, and green spheres represent Zn, O, Co, and Ga atoms, respectively. O atoms which have magnetic moments are labeled 1–7. (b) The total DOS of the atomic configuration (a) with the two Co atoms as ferromagnetic (the upper panel) and antiferromagnetic (the lower panel). (c) The Ga-4p and the Co-3d states in the atomic configuration (a) with the two Co atoms as ferromagnetic (the upper panel) and antiferromagnetic (the lower panel).

simulated. By comparing the total DOS of AFM with that of FM configuration in Fig. 6(b), it is found that for the AFM configuration the system is clearly metallic, and the DOS of the AFM configuration around the Fermi level mainly comes from the Ga-4p states. For the FM configuration, the system is semiconducting with the band gap about 1.5 eV. Ga-4p states are hybridized with Co-3d states from the partial DOS of Co-3d and Ga-4p states [as shown in Fig. 6(b)]. The hybridization causes the delocalization of Co-3d states. By comparing the partial DOS of Co-3d states for the AFM state with FM state, the Co-3d band is more delocalized for the FM. Thus, the kinetic energy is lowered distinctly. Furthermore, it is found that oxygen ions surrounding Ga and Co ions are polarized to different degrees depending on their distances to the Co atoms with the same polarization direction of Co atoms. In Fig. 6(a), the magnetic moments on O1, O2, O3, O4, O5, O6, and O7 atoms are 0.106μ_B, 0.047μ_B, 0.044μ_B, 0.045μ_B, 0.040μ_B, 0.036μ_B, and 0.049μ_B, respectively. This suggests that the magnetic coupling between two Co pairs belonging to different supercells nearby is, most likely, mediated by the delocalization of electronic polarization across O atoms.

The spin-split donor impurity-band model,[18,34,38] which is caused by the strong hybridization between the charge carriers at the Fermi level in the gap, was suggested to explain the high-temperature FM in TM-doped ZnO DMS (e.g., TM =Co). However, in the present case, Co-doped ZnO is non-ferromagnetic at RT. Moreover, no impurity band at the Fermi level in the gap from the partial DOS of Co-3d and Ga-4p states [as shown in Fig. 6(c)] was detected. Thus, we believe that the spin-split donor impurity band cannot be the origin of FM in present studied samples. Based on our experimental and first-principles calculation results, we suggest that the hybridization between the Ga-4p and Co-3d states and O vacancies act as a catalyst for the indirect ferromagnetic exchange interaction between two magnetic ions (Co

ions here). Furthermore, one magnetic ion (Co ions here) pair is ferromagnetically coupled with surrounding magnetic ion (Co ions here) pair, mediated by the delocalization of electronic polarization across O ions. Finally, (Co, Ga)-codoped ZnO sample becomes diluted strong ferromagnetic semiconductor.

IV. CONCLUSIONS

The origin of high-temperature ferromagnetism in (Co, Ga)-codoped ZnO has been investigated. It is found that atomic and electronic structures of Co ions in Co-doped ZnO are modified by doping Ga ions. High temperature (above room temperature) ferromagnetism is observed in $Zn_{0.92}Co_{0.05}Ga_{0.03}O$ sample while nonmagnetic behavior down to 5 K is detected in $Zn_{0.95}Co_{0.05}O$ sample. Co ions with two plus valences and high-spin state prefer to substitute Zn ions in both $Zn_{0.95}Co_{0.05}O$ and $Zn_{0.92}Co_{0.05}Ga_{0.03}O$ samples. The Ga dopant with three plus valences are located at octahedral interstitial site together with one O vacancy, surrounding Co ions. Results obtained here from both experimental studies and first-principles calculations for $Zn_{0.92}Co_{0.05}Ga_{0.03}O$ sample reveal (1) electron transformation from the Ga 4$p^{\uparrow}$ states to the unfilled Co 3$d^{\downarrow}$ states, (2) strong hybridization between the charge carriers in the Co 3d and Ga 4p states, and (3) electronic polarization for surrounding O ions at Co ions. The Ga-4p electrons merged with conduction band, and polarized oxygen ions act as bridge and/or medium for an indirect ferromagnetic exchange interaction between Co pairs, resulting in the ferromagnetism for the (Co, Ga)-codoped ZnO sample.

---

*Author to whom correspondence should be addressed; jiangjz@zju.edu.cn

[1] T. Dietl, H. Ohno, F. Matsukura, J. Cibert, and D. Ferrand, Science **287**, 1019 (2000).

[2] Y. Matsumoto, M. Murakami, T. Shono, T. Hasegawa, T. Fukumura, M. Kawasaki, P. Ahmet, T. Chikyow, S. Koshihara, and H. Koinuma, Science **291**, 854 (2001).

[3] P. Sharma, A. Gupta, K. V. Rao, F. J. Owens, R. Sharma, R. Ahuja, J. M. Osorio, G. B. Johansson, and G. A. Gehring, Nature Mater. **2**, 673 (2003).

[4] J. Philip, A. Punnoose, B. I. Kim, K. M. Reddy, S. Layne, J. O. Holmes, B. Satpati, P. R. Leclair, T. S. Santos, and J. S. Moodera, Nature Mater. **5**, 298 (2006).

[5] A. Sundaresan, R. Bhargavi, N. Rangarajan, U. Siddesh, and C. N. R. Rao, Phys. Rev. B **74**, 161306(R) (2006).

[6] M. A. Garcia, J. M. Merino, E. F. Pinel, A. Quesada, J. D. Venta, R. Gonzalez, G. Castro, P. Crespo, J. Liopis, J. M. Gonzalez-Calbet, and A. Hernando, Nano Lett. **7**, 1489 (2007).

[7] K. Ueda, H. Tabata, and T. Kawai, Appl. Phys. Lett. **79**, 988 (2001).

[8] H. J. Lee, S. Y. Jeong, C. R. Cho, and C. H. Park, Appl. Phys. Lett. **81**, 4020 (2002).

[9] S. G. Yang, A. B. Pakhomov, S. T. Hung, and C. Y. Wong, IEEE Trans. Magn. **38**, 2877 (2002).

[10] J. H. Kim, H. Kim, D. Kim, Y. E. Ihm, and W. K. Choo, Physica B (Amsterdam) **327**, 304 (2003).

[11] Z. G. Yin, N. F. Chen, C. L. Chai and F. Yang, J. Appl. Phys. **96**, 5093 (2004).

[12] Y. B. Zhang, Q. Liu, T. Sritharan, C. L. Gan, and S. Li, Appl. Phys. Lett. **89**, 042510 (2006).

[13] C. Song, K. W. Geng, F. Zeng, X. B. Wang, Y. X. Shen, F. Pan, Y. N. Xie, T. Liu, H. T. Zhou, and Z. Fan, Phys. Rev. B **73**, 024405 (2006).

[14] Z. Jin, T. Fukumura, M. Kawasaki, K. Ando, H. Saito, T. Sekiguchi, Y. Z. Yoo, M. Murakami, Y. Matsumoto, T. Hasegawa, and H. Koinuma, Appl. Phys. Lett. **78**, 3824 (2001).

[15] J. H. Kim, H. Kim, D. Kim, Y. E. Ihm, and W. K. Choo, J. Appl. Phys. **92**, 6066 (2002).

[16] S. W. Yoon, S. B. Cho, S. C. We, S. Yoon, and B. J. Suh, J. Appl. Phys. **93**, 7879 (2003).

[17] N. Khare, M. J. Kappers, M. Wei, M. G. Blamire, and J. L. MacManus-Driscoll, Adv. Mater. (Weinheim, Ger.) **18**, 1449 (2006).

[18] J. M. D. Coey, M. Venkatesan, and C. B. Fitzgerald, Nature Mater. **4**, 173 (2005).

[19] M. H. F. Sluiter, Y. Kawazoe, P. Sharma, A. Inoue, A. R. Raju, C. Rout, and U. V. Waghmare, Phys. Rev. Lett. **94**, 187204 (2005).

[20] X. C. Liu, E. W. Shi, Z. Z. Chen, H. W. Zhang, B. Xiao, and L. X. Song, Appl. Phys. Lett. **88**, 252503 (2006).

[21] K. R. Kittilstved, D. A. Schwartz, A. C. Tuan, S. M. Heald, S. A. Chambers, and D. R. Gamelin, Phys. Rev. Lett. **97**, 037203 (2006).

[22] J. R. Neal, A. J. Behan, R. M. Ibrahim, H. J. Blythe, M. Ziese, A. M. Fox, and G. A. Gehring, Phys. Rev. Lett. **96**, 197208 (2006).

[23] X. H. Xu, H. J. Blythe, M. Ziese, A. J. Behan, J. R. Neal, A. Mokhtari, R. M. Ibrahim, A. M. Fox, and G. A. Gehring, New J. Phys. **8**, 135 (2006).

[24] X. J. Liu, C. Song, F. Zeng, and F. Pan, J. Phys.: Condens. Matter **19**, 296208 (2007).

[25] J. Alaria, H. Bieber, S. Colis, G. Schmerber, and A. Dinia, Appl. Phys. Lett. **88**, 112503 (2006).

[26] A. J. Behan, A. Mokhtari, H. J. Blythe, D. Score, X. H. Xu, J. R. Neal, A. M. Fox, and G. A. Gehring, Phys. Rev. Lett. **100**, 047206 (2008).

[27] S. Yin, M. X. Xu, L. Yang, J. F. Liu, H. Rosner, H. Hahn, H. Gleiter, D. Schild, S. Doyle, T. Liu, T. D. Hu, E. Takayama-Muromachi, and J. Z. Jiang, Phys. Rev. B **73**, 224408 (2006).

[28] A. L. Ankudinov and J. J. Rehr, Phys. Rev. B **62**, 2437 (2000).

[29] P. E. Blöchl, Phys. Rev. B **50**, 17953 (1994).

[30] G. Kresse and J. Furthmüller, Phys. Rev. B **54**, 11169 (1996); Comput. Mater. Sci. **6**, 15 (1996); G. Kresse and D. Joubert, Phys. Rev. B **59**, 1758 (1999).

[31] V. Anisimov, F. Aryasetiawan, and A. Lichtenstein, J. Phys.: Condens. Matter **9**, 767 (1997).

[32] T. Chanier, M. Sargolzaei, I. Opahle, R. Hayn, and K. Koepernik, Phys. Rev. B **73**, 134418 (2006).

[33] J. F. Moulder, W. F. Stickle, P. E. Sobol, and K. D. Bomben, in *Handbook of X-Ray Photoelectron Spectroscopy*, edited by J. Chastain (Perkin-Elmer, Eden Prairie, MN, 1992), p. 83.

[34] X. F. Wang, J. B. Xu, B. Zhang, H. G. Yu, J. Wang, X. X. Zhang, J. G. Yu, and Q. Li, Adv. Mater. (Weinheim, Ger.) **18**, 2476 (2006).

[35] Z. P. Fu, B. F. Yang, L. Li, W. W. Dong, C. Jia, and W. Wu, J. Phys.: Condens. Matter **15**, 2867 (2003).

[36] G. Schön, J. Electron Spectrosc. Relat. Phenom. **2**, 75 (1973).

[37] FEFF is a program for *ab initio* multiple-scattering calculations of XAFS and x-ray absorption near-edge structure spectra for clusters of atoms. The code yields scattering amplitudes and phases used in many modern XAFS analysis codes, as well as various other properties.

[38] M. Venkatesan, C. B. Fitzgerald, J. G. Lunney, and J. M. D. Coey, Phys. Rev. Lett. **93**, 177206 (2004).